ISSN 0036-0244, Russian Journal of Physical Chemistry A, 2014, Vol. 88, No. 7, pp. 1147–1157. © Pleiades Publishing, Ltd., 2014.

STRUCTURE OF MATTER AND QUANTUM CHEMISTRY

A Theoretical Study on Tautomeric Structures of 4'-Nitroazobenzene-2,4-diol and 4-Methyl-4'-nitroazobenzene-2,6-diol Compounds[1]

M. Karakaya[a,*] and F. Ucun[b]

[a] *Department of Energy Systems, Faculty of Engineering and Architecture, Sinop University, 57000 Sinop, Turkey*

[b] *Department of Physics, Faculty of Arts and Sciences, Süleyman Demirel University, 32260 Isparta, Turkey*

**e-mail: mkarakayafizik@hotmail.com*

Received August 6, 2013

Abstract—The goal of this study is to determine the most stable tautomeric forms, and their ground state conformers of 4'-nitroazobenzene-2,4-diol and 4-methyl-4'-nitroazobenzene-2,6-diol compounds. The calculations have shown that the most stable tautomeric forms of the compounds are hydrazo form for 4'-nitroazobenzene-2,4-diol and azo form for 4-methyl-4'-nitroazobenzene-2,6-diol. Besides, the vibrational frequencies, ^{1}H and ^{13}C NMR shifts, frontier molecular orbital's energies for the tautomeric forms of the compounds calculated by using density functional theory-B3LYP method with 6-311G(*d*) basis set were interpreted. All the assignments of the theoretical frequencies were identified by potential energy distribution (PED) analysis. Generally, theoretical spectral results were seen to be in a good agreement with the corresponding experimental data.

Keywords: 4'-nitroazobenzene-2,4-diol, 4-methyl-4'-nitroazobenzene-2,6-diol, IR spectra, NMR spectra, density functional theory (DFT).

DOI: 10.1134/S003602441407022X

1. INTRODUCTION

Azobenzene derivatives are not only used as dyestuffs but also as data storage materials in recently developing optical devices [1–5]. They carry remarkable isomerization properties with two stable conformers (*trans* and *cis*) easily accessible through appropriate photon absorption [6]. A mechanism for the thermal *cis–trans* isomerization of azobenzenes has extensively been studied, and the effect of substituents, solvent polarity and pressure has been discussed [7]. The combined NMR and electronic spectroscopic studies have carried out on tautomeric structures of azobenzene derivatives [8]. Tautomeric forms of diazo dyes have different colors, tinctorial strengths and different properties, e.g., light fastness. Gup and et al. have investigated the tautomeric structure of barbituric acid dyes in the solid and liquid state by using FT-IR [9]. They have found that diazo dyes exit in triketo forms in solid state while they are in azo-enol forms in solution [10].

Similar materials have been studied by density functional theory and different experimental methods in the recent past [11–13]. In the present study the most stable tautomeric forms of 4'-nitroazobenzene-2,4-diol (*NAB*-1), also known as magneson, and 4-methyl-4'-nitroazobenzene-2,6-diol (*NAB*-2) compounds were identified and the calculated vibrational frequencies, ^{1}H and ^{13}C NMR shift values of their designed most stable conformers were compared with the corresponding experimental data.

2. COMPUTATIONAL DETAILS

The vibrational frequencies of *NAB*-1 and *NAB*-2 compounds were calculated by density functional theory-B3LYP method at 6-311G(*d*) basis set level and then the theoretical vibration frequencies were scaled with a scale factor of 0.9614 [14]. The ^{1}H and ^{13}C NMR chemical shifts (in DMSO solvent and solvent free) were done by Gauge Including Atomic Orbitals (GIAO) method, and the solvent effects were taken into account by means of the PCM approximation using 6-311G(*d*) basis set of the theory which is routinely used for NMR chemical shift calculations [15, 16]. In the chemical shift calculations tetramethylsilane (TMS) was used as a reference molecule, and the theoretical chemical shift ^{1}H and ^{13}C values were obtained by subtracting the GIAO isotropic magnetic shielding (IMS) values [17, 18]. All these computations were done by using Gaussian 03 software package [19] on the personal computer. The assignments of the theoretical frequencies were identified by means of the potential energy distribution (PED) analysis using

[1] The article is published in the original.

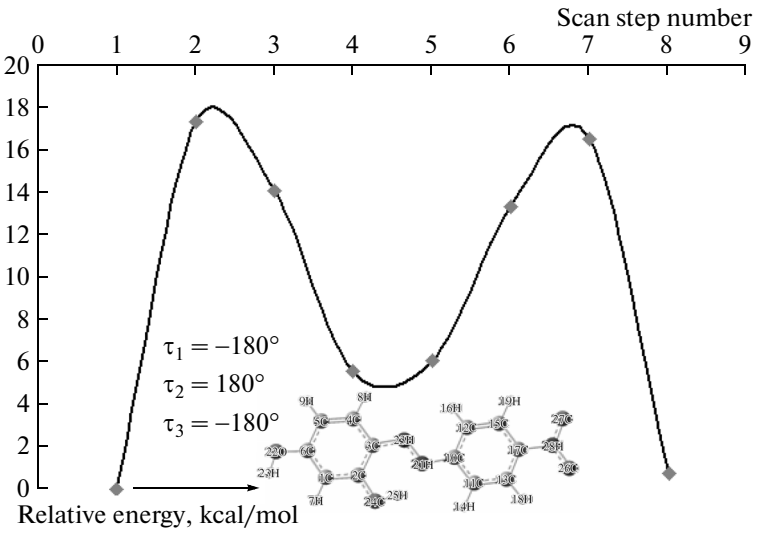

Fig. 1. The graph for potential energy surface scan of *NAB*-1. Figure note: [step number; τ_1, τ_2, τ_3 (deg)] = [1; −180°, 180°, −180°], [2; 180°, 0°, −180°], [3; 180°, 0°, 0°], [4; 180°, 180°, 0°], [5; 0°, 180°, 0°], [6; 0°, 0°, 0°], [7; 0°, 0°, −180°], [8; 0°, 180°, −180°].

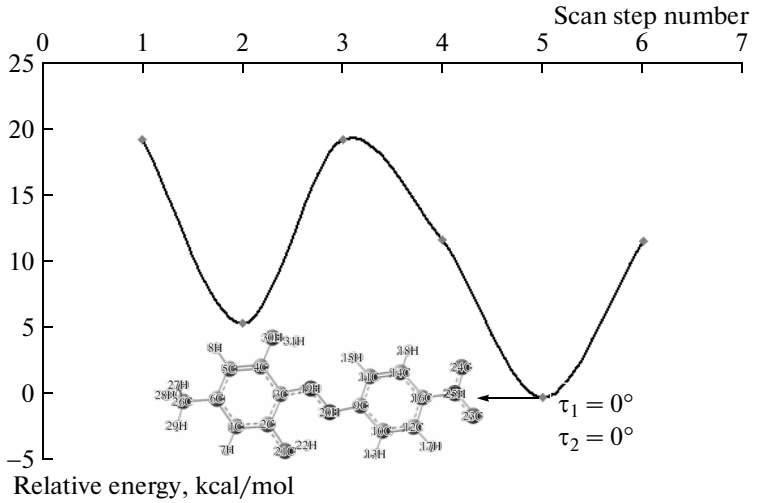

Fig. 2. The graph for potential energy surface scan of *NAB*-2. Figure note: [step number; τ_1, τ_2, (deg)] = [1; 180°, −180°], [2; 180°, 0°], [3; 180°, −180°], [4; 0°, 0°], [5; 0°, 0°], [6; 180°, −180°].

VEDA 4 program [20], and these vibration modes were supported by using Gauss-View molecular visualization programs [21]. For locating transition structures the *Synchronous Transit-Guided Quasi-Newton* (STQN) Method, developed by H.B. Schlegel and coworkers, uses a linear synchronous transit to get closer to the quadratic region around the transition state and then uses a quasi-Newton or eigenvector- following algorithm to perform the optimization [22, 23]. *Quantum Synchronous Transit2* (QST2) option is used requested by this method. To find the optimum transition states of these compounds, QST2 (Quantum Synchronous Transit2) approaches were used by taking their optimized azo and hydrazo forms in our study.

3. RESULTS AND DISCUSSION

3.1. Ground State Conformer Analysis

Firstly, in order to find the minimal energy conformers of *NAB*-1, a detailed potential energy surface (PES) scans were simultaneously performed on τ_1[5C–6C–22O–23H], τ_2 [1C–2C–24O–25H], and τ_3[4C–3C–20N–21N] torsion angles. Similarly, τ_1[3C–4C–30O–31H] and τ_2[3C–2C–21O–22H] torsion angles were used for the *NAB*-2 molecule, simultaneously. These scans were done for −180°, 0°, 180° values (in 8 steps for *NAB*-1 and 6 steps for *NAB*-2) on the each torsion angles in order to find the minimizing the potential energy. All of PES scans were performed by density functional theory-B3LYP method

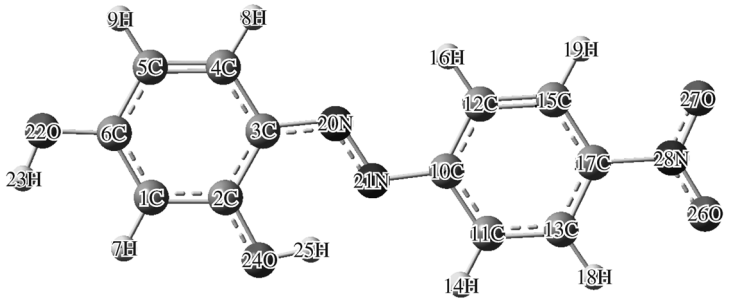

Fig. 3. Optimize molecular structure of *NAB*-1 by using 6-311G(*d*) basis set at DFT method.

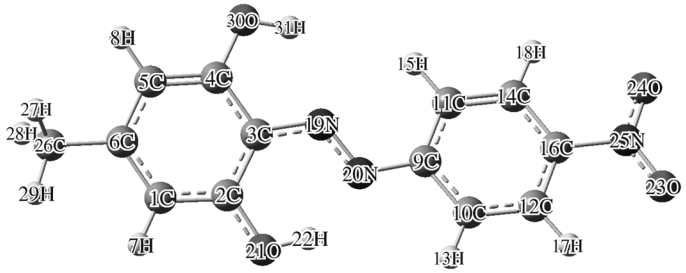

Fig. 4. Optimize molecular structure of *NAB*-2 by using 6-311G(*d*) basis set at DFT method.

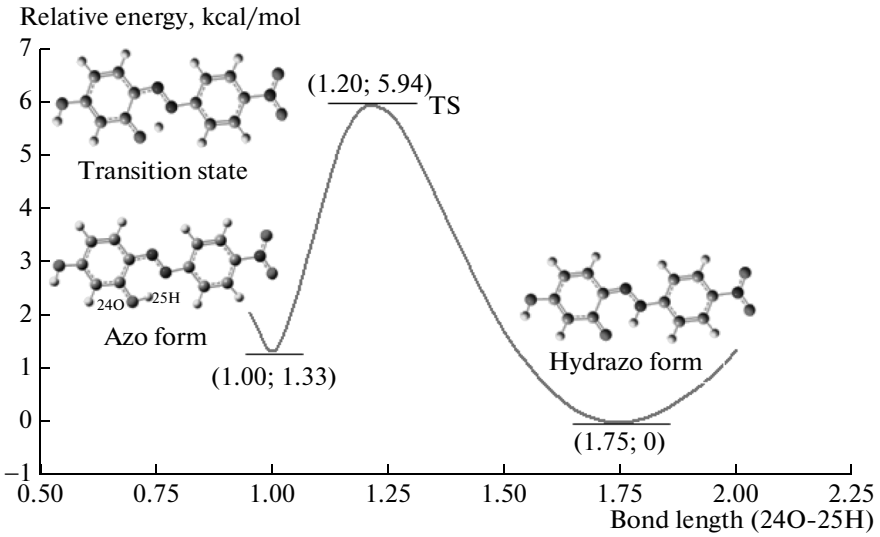

Fig. 5. PES scan graph for azo, hydrazo and TS form of *NAB*-1.

at 6-31G basis set level. The graphs of the PES scans and minimum energy structures with the essential torsion angles values of the title compounds are given Figs. 1 and 2.

After scanning the designed minimum energy structures were optimized by DFT–B3LYP method at 6-311G(*d*) basis set. These structures with the atom numberings are shown in Figs. 3 and 4. For *NAB*-1 sums of electronic and zero-point energy (ZPE) are –927.731, –927.729, and –927.733 Hartree/part for its azo, TS and hydrazo form, respectively, and for *NAB*-2, –967.033, –967.028, and –967.032 Hartree/part for its azo, TS, and hydrazo forms. If the energy values are carefully analyzed, it can be seen that the minimal energy structures are hydrazo form for *NAB*-1 and azo form for *NAB*-2. Molecular weights of *NAB*-1 ($C_{12}H_9N_3O_4$) and *NAB*-2 ($C_{13}H_{11}N_3O_4$) are 259.22 and 273.20 g mol^{-1}, respectively and the melt-

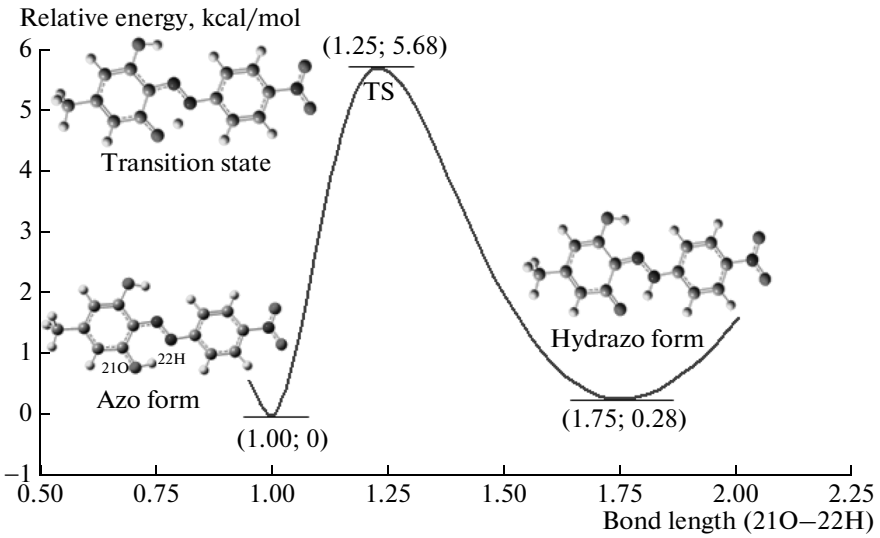

Fig. 6. PES scan graph for azo, hydrazo and TS form of *NAB*-2.

ing point range for *NAB*-1 compound is given as 195–200°C in literature [24, 25].

3.2. Tautomeric Forms

The potential energy surface (PES) scans were done by changing of the bond lengths 24O–25H for *NAB*-1 and 21O–22H for *NAB*-2 from 0.95 to 2.00 Å in steps of 0.05 Å using density functional theory–B3LYP method at 6-311G(*d*) basis set level. These results were given in Figs. 5 and 6, respectively. As also seen from the figures the hydrazo form for *NAB*-1 and azo form for *NAB*-2 are more stable. The relative and barier energy values between the azo and hydrazo forms are 1.33, 5.94 kcal/mol for the *NAB*-1 and 0.28, 5.68 kcal/mol for the *NAB*-2, respectively. Frontier molecular orbitals (FMO's) are important in determining such properties as molecular reactivity and the ability of a molecule to absorb light. FMO's are also very important for optical and electric properties [26]. The highest occupied molecular orbital (HOMO) and the lowest unoccupied molecular orbital (LUMO) are the main orbital taking part in chemical reaction. The HOMO energy characterizes the ability of electron giving, the LUMO energy characterizes the ability of electron accepting, and the gap between HOMO and LUMO energies characterizes the molecular chemical stability [27]. The HOMO–LUMO gap is also called the "band gap." It refers to the potential energy difference between the highest occupied molecular orbital (HOMO) and the lowest unoccupied molecular orbital (LUMO). Fundamentally, it is how much energy we have to feed into the molecule to kick it from the ground (most stable) state into an excited state. For example, a small band gap means we don't need as much energy to excite the molecule. We computed the frontier molecular orbital's energies at B3LYP/6-311 G(*d*) level for all the tautomeric forms of the compounds (Table 1). As shown from Table 1, the minimal E_g (band gap) values belong to the hydrazo forms for *NAB*-1 and *NAB*-2. Minimal HOMO–LUMO gap for *NAB*-1 supports results of scan graph in Fig. 5.

3.3. Vibration Frequencies and Assignments

The resulting vibration frequencies for all the forms of the title compounds are given in Tables 2 and 3. For comparison, the experimental vibration frequencies (IR) of the compounds are also given in the tables [24]. As realized from Fig. 3, the *NAB*-1 molecule is planar and belongs to the C_s point group. So, the vibrations being symmetric through the mirror plane σ_h will belong to the species A', and the ones being anti-symmetric to the species A". The numbers of vibration modes are $\Gamma_{vib} = 53A' + 25A''$. *NAB*-2 is non-planar

Table 1. The frontier and second frontier molecular orbital's energy levels (eV) for azo and hydrazo forms of the title compounds

	NAB-1		*NAB*-2	
	azo form	hydrazo form	azo form	hydrazo form
LUMO + 1	–2.07	–2.25	–2.22	–2.39
LUMO	–3.21	–3.25	–3.39	–3.41
HOMO	–6.46	–6.37	–6.50	–6.18
HOMO – 1	–7.12	–7.00	–6.73	–6.97
E_g	3.25	3.12	3.11	2.77

E_g = [HOMO – LUMO].

Table 2. Experimental and calculated vibrational frequencies, their symmeries and assignments of *NAB*-1

Mode no.	Symmetry	Calculated frequencies (cm^{-1}) DFT/B3LYP method 6-311G(*d*) basis set			Experimental[a] IR (solid sample, KBr disc) frequencies (cm^{-1}) azo form	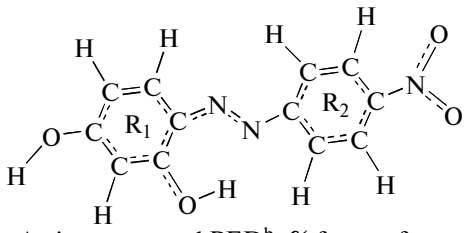 Assignments and PED[b], % for azo form
		azo form	transition state	hydrazo form		
78	*A*'	3637	3632	3629	3418br	$\nu_{OH}(100)$(4-hydroxy)
77	*A*'	3108	3108	3110	3115w	$R_2[\nu_{CH}(100)$ sym]
76	*A*'	3107	3107	3107		$R_2[\nu_{CH}(77)$ asym]
75	*A*'	3096	3095	3105		$R_2[\nu_{CH}(98)$ asym]
74	*A*'	3089	3090	3098		$R_1[\nu_{CH}(95)$ sym]
73	*A*'	3078	3071	3088	3094br	$\nu_{OH}(92)$(2-hydroxy)
72	*A*'	3073	3068	3069	3080br	$R_1[\nu_{CH}(95)$ asym]
71	*A*'	3071	3051	3060	2750br	$R_2[\nu_{CH}(95)$ asym]
70	*A*'	3051	1838	3048	2655br	$R_1[\nu_{CH}(97)]$
69	*A*'	1613	1604	1625	1632s	$R_1[\nu_{CC}(56) + \delta_{HCC}(12)]$
68	*A*'	1586	1586	1589	1606s	$R_1[\nu_{CC}(56)] + \nu_{ON(}25)$
67	*A*'	1577	1578	1582	1595s	$R_2[\nu_{CC}(26) + \delta_{HCC}(16)]$
66	*A*'	1564	1531	1573		$R_1[\nu_{CC}(29) + \delta_{HOC}(21)]$
65	*A*'	1532	1520	1535		$R_2[\nu_{ON}(60) + \nu_{CC}(15)]$
64	*A*'	1494	1505	1524	1511vs	$R_1[\delta_{HCC}(26) + \delta_{HOC}(22) + \nu_{CC}(20)]$
63	*A*'	1477	1472	1520		$\nu_{NN}(20) + R_1[\delta_{HCC}(12)]$
62	*A*'	1460	1459	1477	1464s	$R_2[\delta_{HCC}(49) + \nu_{CC}(12)]$
61	*A*'	1407	1407	1454		$R_2[\delta_{HCC}(17)] + \nu_{NN}(16) + R_1[\nu_{CC}(12)]$
60	*A*'	1406	1365	1411	1403m	$R_1[\delta_{HOC}(30) + \nu_{CC}(27) + \delta_{HCC}(10)]$
59	*A*'	1371	1359	1386	1397m	$\nu_{NN}(40) + R_1[\nu_{CC}(13)]$
58	*A*'	1322	1333	1346	1389sh	$\nu_{ON}(55)$
57	*A*'	1321	1311	1319	1340vs	$R_2[\nu_{CC}(28)] + R_1[\nu_{CC}(17)]$
56	*A*'	1308	1306	1312		$R_2[\nu_{CC}(26)] + R_1[\nu_{OC}(11)]$
55	*A*'	1304	1290	1287		$\nu_{ON}(12)$
54	*A*'	1273	1278	1273	1261s	$R_2[\delta_{HCC}(79)]$
53	*A*'	1248	1233	1248		$(R_1 + R_2)[\nu_{NC}(48)]$
52	*A*'	1210	1208	1215	1226s	$R_1[\delta_{HCC}(20) + \delta_{HOC}(14)]$
51	*A*'	1186	1197	1187	1204sh	$R_1[\nu_{OC}(49) + \delta_{HCC}(22)]$
50	*A*'	1178	1160	1183		$(R_1 + R_2)[\nu_{NC}(25)]$
49	*A*'	1154	1148	1158	1162s	$R_1[\delta_{HOC}(31) + \delta_{HCC}(17)]$
48	*A*'	1136	1132	1150	1126sh	$R_2[\delta_{HCC}(49)] + (R_1 + R_2)[\nu_{NC}(10)]$
47	*A*'	1097	1104	1108	1115m	$R_1[\delta_{HCC}(55) + \nu_{CC(}12)]$
46	*A*'	1086	1090	1092	1110s	$R_2[\delta_{HCC}(66)]$
45	*A*'	1077	1080	1081		$R_2[\nu_{CC}(40) + \nu_{NC}(23)]$
44	*A*'	985	986	985		$(R_1 + R_2)[\delta_{CCC}(59)] + R_2[\delta_{HCC}(21)]$
43	*A*''	970	964	960	965w	$R_2[\tau_{HCCC}(82)]$
42	*A*'	954	951	941		$R_1[\nu_{CC}(25) + \delta_{HCC}(13) + \nu_{OC}(10) + \delta_{CCC}(10)]$
41	*A*''	948	945	938		$R_2[\tau_{HCCC}(84)]$
40	*A*''	924	933	929		$R_1[\tau_{HCCC}(87)]$
39	*A*'	903	924	861		$R_2[\delta_{NNC}(18) + \nu_{CC}(12)] + R_1[\delta_{CNN}(18)]$
38	*A*''	855	846	851	855s	$R_2[\tau_{HCCC}(70) + \gamma_{NCCC}(12)]$
37	*A*'	840	839	838	846s	$\delta_{ONO}(44) + R_2[\nu_{CC}(14)] + \nu_{ON}(13)$

Table 2. (Contd.)

Mode no.	Symmetry	Calculated frequencies (cm^{-1}) DFT/B3LYP method 6-311G(*d*) basis set			Experimental[a] IR (solid sample, KBr disc) frequencies (cm^{-1}) azo form	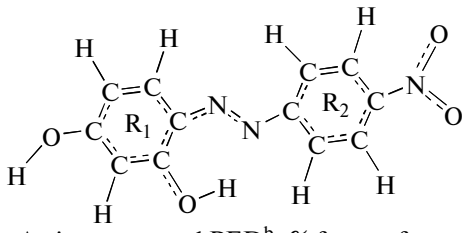 Assignments and PED[b], % for azo form
		azo form	transition state	hydrazo form		
36	*A*''	816	808	832		$R_2[\tau_{HCCC}(86)]$
35	*A*''	805	799	805	809sh	$R_1[\tau_{HCCC}(30) + \tau_{HOCC}(10) + \gamma_{OCCC}(20)]$
34	*A*''	795	799	797	799m	$R_1[\tau_{HOCC}(55)]$
33	*A*'	794	788	790		$R_1[\delta_{CCC}(22)] + (R_1 + R_2)[\nu_{NC}(18)] + \delta_{ONO}(11)$
32	*A*''	792	727	782	760m	$R_1[\tau_{HCCC}(64) + \gamma_{OCCC}(12)]$
31	*A*''	730	726	722	732sh	$R_2[\gamma_{OCON}(41) + \gamma_{NCCC}(14)]$
30	*A*'	728	707	707		$R_1[\delta_{CCC}(51) + \nu_{CC}(13) + \nu_{OC}(12)]$
29	*A*''	698	686	702		$R_1[\tau_{HCCC}(26) + \tau_{CCCC}(23) + \gamma_{OCCC}(17)]$
28	*A*''	677	677	677	687m	$R_2[\gamma_{OCON}(30) + \tau_{CCCC}(15) + \tau_{HCCC}(12)]$
27	*A*'	670	643	661		$R_2[\delta_{CCC}(19) + \nu_{NC}(10)] + \delta_{ONO}(17)$
26	*A*''	635	625	642	638w	$R_1[\gamma_{OCCC}(55) + \tau_{HCCC}(19)]$
25	*A*'	624	596	624	613m	$R_2[\delta_{CCC}(36) + \nu_{CC}(11) + \delta_{NCC}(11)]$
24	*A*'	587	564	591		$R_1[\delta_{CCN}(22) + \delta_{OCC}(14)]$
23	*A*'	532	530	522	536m	$R_1[\delta_{HCC}(26) + \delta_{HOC}(22) + \nu_{CC}(20) + \delta_{CCC}(15)] + R_2[\nu_{NC}(11)]$
22	*A*'	521	522	517	516w	$R_2[\delta_{ONC}(36) + \delta_{NCC}(10)] + (R_1 + R_2)\delta_{CCC}(14)$
21	*A*''	509	502	499	503w	$R_2[\gamma_{NCCC}(39)] + (R_1 + R_2)[\tau_{CNNC}(13) + \tau_{CCCC}(12)]$
20	*A*'	496	496	493		$R_1[\delta_{OCC}(20)] + R_2[\delta_{ONC}(19)]$
19	*A*'	455	458	479		$R_1[\delta_{OCC}(41)] + R_2[\delta_{NCC}(11)]$
18	*A*''	450	442	452		$(R_1 + R_2)[\tau_{CCCC}(35)] + R_1[\gamma_{OCCC}(20) + \tau_{HCCC}(11)]$
17	*A*''	427	414	438		$R_1[\tau_{HOCC}(92)]$
16	*A*''	408	413	414		$R_2[\tau_{CCCC}(54) + \tau_{HCCC}(21)]$
15	*A*''	393	406	407		$(R_1 + R_2)[\tau_{CCCC}(38) + \tau_{CNNC}(12)] + R_1[\gamma_{OCCC}(13)]$
14	*A*'	391	387	386		$R_2[\nu_{NC(}27) + \delta_{CCC}(17)]$
13	*A*'	345	343	367		$R_1[\delta_{OCC}(65)]$
12	*A*''	330	301	318		$R_2[\tau_{CCCC}(17) + \gamma_{NCCC}(16)] + R_1[\tau_{CCNN}(12)]$
11	*A*'	291	253	289		$R_2[\delta_{NCC}(28) + \delta_{ONC}(12)] + R_1[\delta_{CCN}(21)]$
10	*A*''	237	209	246		$R_1[\tau_{CCNN}(36) + \gamma_{OCCC}(15)] + (R_1 + R_2)[\tau_{CCCC}(12)]$
09	*A*''	213	208	205		$R_1[\tau_{CCCC}(33) + \tau_{CCCN}(21) + \gamma_{OCCC}(12)]$
08	*A*'	206	197	188		$R_2[\delta_{NNC}(24)] + (R_1 + R_2)[\nu_{NC}(11)]$
07	*A*'	172	164	172		$R_2[\delta_{NCC}(26)] + (R_1 + R_2)[\nu_{NC}(15)] + R_1[\delta_{CNN}(13) + \delta_{CCN}(10)]$
06	*A*''	168	83	151		$(R_1 + R_2)[\tau_{CCCC}(28)] + \tau_{CNNC}(19) + R_2[\gamma_{NCCC}(14)]$
05	*A*''	81	63	76		$(R_1 + R_2)[\tau_{CCCC}(52)] + \tau_{CNNC}(15)$
04	*A*'	60	59	64		$R_2[\delta_{NNC}(34) + \delta_{NCC}(21)] + R_1[\delta_{CNN}(23)]$
03	*A*''	56	32	58		$R_2[\tau_{ONCC}(91)]$
02	*A*''	32	28	38		$\tau_{CNNC}(35) + R_2[\gamma_{NCCC}(17)] + (R_1 + R_2)[\tau_{CCCC}(10)]$
01	*A*''	23		28		$R_2[\tau_{NNCC}(65)] + R_1[\tau_{CCNN}(10)]$
	$R^2 =$	0.991	0.966	0.992		
	RMSD =	95.37	152.73	92.78		

[a] Taken from [24].
[b] Potential energy distribution (PED) less than 10% are not shown.
ν, stretching; δ, bending; γ, out of plane bending; τ, torsion modes; sym, symmetric; asym, anti symmetric; w, weak; m, medium; s, strong; v, very; sh, shoulder; br, broad.

Table 3. Experimental and calculated vibrational frequencies, their assignments of *NAB*-2

Mode no.	Calculated frequencies (cm^{-1}) DFT/B3LYP method 6-311G(*d*) basis set			Experimental[a] IR (solid sample, KBr disc) frequencies (cm^{-1}) azo form	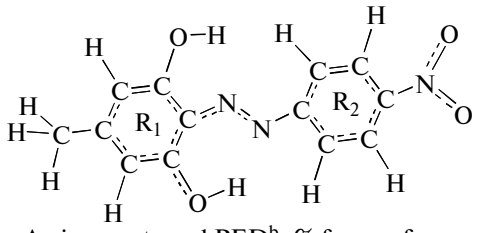 Assignments and PED[b], % for azo form
	azo form	transition state	hydrazono form		
87	3519	3548	3551		$\nu_{OH}(100)$(6-hydroxy)
86	3155	3108	3110		$\nu_{OH}(98)$(2-hydroxy)(O–H···N)
85	3108	3107	3107		$R_2[\nu_{CH}(100)$ sym]
84	3107	3095	3101		$R_2[\nu_{CH}(94)$ asym]
83	3094	3074	3097		$R_2[\nu_{CH}(96)$ asym]
82	3072	3071	3071		$R_2[\nu_{CH}(96)$ asym]
81	3072	3070	3069		$R_1[\nu_{CH}(95)$ sym]
80	3070	3001	3062		$R_1[\nu_{CH}(100)$ asym]
79	3000	2961	3003	2966sh	Me[$\nu_{CH}(89)$ asym]
78	2964	2916	2957	2927vs	Me[$\nu_{CH}(95)$ asym]
77	2918	1845	2913	2855vs	Me[$\nu_{CH}(98)$ sym]
76	1627	1622	1642	1629w	$R_1[\nu_{CC}(46) + \delta_{HOC}(15)]$
75	1586	1586	1593	1594m	$R_2[\nu_{CC}(40)] + \nu_{ON}(27)$
74	1577	1577	1582		$R_2[\nu_{CC}(26)]$
73	1545	1532	1576		$R_1[\nu_{CC}(25) + \delta_{HOC}(17) + \delta_{CCC}(13)]$
72	1532	1512	1541	1510br	$\nu_{ON}(27) + R_2[\nu_{CC}(17)]$
71	1487	1494	1530		$R_1[\nu_{CC}(25) + \delta_{HOC}(23) + \delta_{HCC}(17)]$
70	1473	1472	1501		$\nu_{NN}(12) + R_1[\nu_{OC}(11)]$
69	1462	1455	1477	1468s	$R_2[\delta_{HCC}(51) + \nu_{CC}(11)]$
68	1449	1442	1446		Me[$\delta_{HCH}(55) + \tau_{HCCC}(10)$] + $R_1[\delta_{HOC}(10)]$
67	1444	1435	1441		Me[$\delta_{HCH}(75)$] + (Me + R_1)[$\tau_{HCCC}(12)$]
66	1418	1406	1433	1412sh	$\nu_{NN}(40)$
65	1392	1388	1415		$\nu_{NN}(11) + R_2[\nu_{CC}(11)]$
64	1377	1371	1389	1377w	Me[$\delta_{HCH}(23)$] + $R_1[\delta_{HOC}(20) + \nu_{CC}(11)]$
63	1372	1360	1374	1338s	Me[$\delta_{HCH}(62)$]
62	1336	1336	1348		$R_1[\nu_{OC}(19) + \nu_{CC}(10)]$
61	1322	1310	1321		$\nu_{ON}(54) + \delta_{ONO}(10)$
60	1311	1306	1313		$R_2[\nu_{CC}(11)]$
59	1290	1296	1286		$(R_1 + R_2)[\nu_{CC}(18)] + R_1[\delta_{HCC}(10)]$
58	1275	1278	1272		$R_2[\delta_{HCC}(73)]$
57	1268	1236	1261	1267sh	$(R_1 + R_2)[\nu_{NC}(33)] + R_1[\nu_{CC}(12)]$
56	1227	1219	1223	1222w	$R_1[\delta_{HOC}(17) + \delta_{HCC}(11) + \nu_{CC}(11)] + (R_1 + R_2)[\nu_{NC}(16)]$
55	1194	1211	1217	1208m	$R_1[\delta_{HCC}(39) + \nu_{OC}(24)]$
54	1179	1149	1181	1166br	$(R_1 + R_2)[\nu_{NC}(32)] + R_2[\delta_{HCC}(13)]$
53	1139	1127	1153	1143m	$R_2[\delta_{HCC}(45)]$
52	1120	1119	1113	1108m	$R_2[\delta_{HCC}(40)] + \nu_{CC}(28)$[Me-$R_1$]
51	1088	1091	1093		$R_2[\delta_{HCC}(70)]$
50	1080	1086	1081		$R_2[\nu_{CC}(30) + \nu_{CN}(19)$C-$NO_2]$
49	1074	1079	1071		$\nu_{OC}(26) + R_2[\nu_{CC}(11)]$
48	1020	1020	1022	1024m	Me[$\tau_{HCCC}(67) + \delta_{HCH}(17)$]
47	985	986	985	989w	Me[$\tau_{HCCC}(35) + \delta_{HCH}(11)$] + $(R_1 + R_2)[\delta_{CCC}(10)]$
46	984	984	984		$(R_1 + R_2)[\delta_{CCC}(22)]$ + Me[$\tau_{HCCC}(22)$]
45	964	964	959		$\nu_{CC}(28)$[Me-R_1] + $\nu_{OC}(10)$
44	960	956	953		$R_2[\tau_{HCCC}(69)]$
43	950	945	942		$R_2[\tau_{HCCC}(88)]$
42	900	931	858		$R_2[\delta_{NCC}(20) + \nu_{CC}(11)] + R_1[\delta_{CNN}(18)]$

Table 3. (Contd.)

Mode no.	Calculated frequencies (cm^{-1}) DFT/B3LYP method 6-311G(*d*) basis set			Experimental[a] IR (solid sample, KBr disc) frequencies (cm^{-1}) azo form	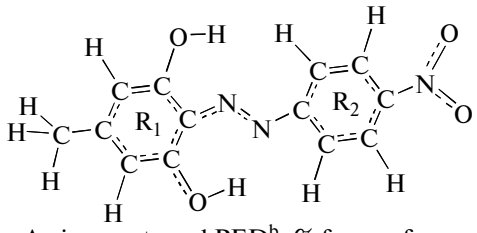 Assignments and PED[b], % for azo form
	azo form	transition state	hydrazono form		
41	850	841	848	866m	$R_2[\tau_{HCCC}(69) + \gamma_{NCCC}(13)]$
40	840	839	831	849m	$R_2[\delta_{ONO}(42) + \nu_{CC}(13)] + \nu_{ON}(11)$
39	826	822	830		$R_1[\tau_{HCCC}(69) + \gamma_{OCCC}(14)]$
38	811	805	824		$R_2[\tau_{HCCC}(95)]$
37	806	804	809		$R_1[\tau_{HCCC}(69) + \gamma_{OCCC}(13)]$
36	795	801	794		$(R_1 + R_2)[\nu_{NC}(17) + \delta_{CCC}(10)] + \delta_{ONO}(12)$
35	767	738	787	771br	$R_1[\tau_{HOCC}(77)]$
34	734	723	736	749m	$R_2[\gamma_{OCON}(28) + \gamma_{NCCC}(10)] + (R_1 + R_2)[\tau_{CCCC}(16)] + R_1[\gamma_{OCCC}(11)]$
33	719	686	721		$R_1[\gamma_{OCCC}(21) + \tau_{HCCC}(11)] + R_2[\gamma_{OCON}(21)] + (R_1 + R_2)[\tau_{CCCC}(15)]$
32	678	676	676		$R_2[\gamma_{OCON}(31) + (\tau_{HCCC}(13)] + (R_1 + R_2)[\tau_{CCCC}(12)]$
31	669	630	661	666br	$R_2[\delta_{CCC}(19)] + \delta_{ONO}(15) + \nu_{CN}(10)$C-$NO_2$
30	626	612	627	627w	$R_2[\delta_{CCC}(29) + \delta_{NCC}(11)]$
29	607	611	608		$R_1[\gamma_{OCCC}(54) + \tau_{HCCC}(18)]$
28	603	578	606		$R_1[\delta_{OCC}(16) + \delta_{CCN}(14)] + (R_1 + R_2)[\delta_{CCC}(14)]$
27	591	573	571	592w-br	$R_1[\tau_{HOCC}(77) + \gamma_{OCCC}(10)]$
26	574	564	564		$R_1[\nu_{OC}(15) + \nu_{CC}(22) + \delta_{CCC}(11)]$
25	571	542	524		$R_1[\gamma_{OCCC}(27) + \tau_{HCCC}(14)]$
24	528	525	518		$R_2[\delta_{ONC}(26)] + (R_1 + R_2)[\delta_{CCC}(14)]$
23	512	510	502		$R_2[\delta_{ONC}(22)] + (R_1 + R_2)[\delta_{CCC}(12)] + R_1[\nu_{NN}(12) + \nu_{OC}(11)]$
22	504	497	490		$R_2[\gamma_{NCCC}(35)] + R_1[\tau_{CCNN}(10)]$
21	501	491	489	497w-br	$R_2[\delta_{HHC}(51) + \nu_{CC}(11)] + R_1[\delta_{OCC}(32) + \delta_{CCC}(23)]$
20	468	428	463		$R_2[\delta_{ONC}(14) + \delta_{NNC}(13)] + (R_1 + R_2)[\delta_{CCC}(12)] + R_1[\delta_{OCC}(11)]$
19	408	413	415		$(R_1 + R_2)[\tau_{CCCC}(34)] + R_2[\gamma_{CCCC}(32) + \tau_{HCCC}(19)]$
18	395	406	407		$(R_1 + R_2)[\delta_{CCC}(21)] + R_2[\nu_{NC}(18)]$
17	394	400	392		$(R_1 + R_2)[\tau_{CCCC}(37)] + \tau_{CNNC}(13)$
16	356	348	375		$R_1[\delta_{OCC}(57)]$
15	334	291	323		$R_1[\tau_{CCNN}(20)] + R_2[\tau_{CCCC}(17) + \gamma_{NCCC}(14)]$
14	288	277	290		$R_1[\delta_{CCC}(52) + \delta_{OCC}(17)]$
13	277	258	275		$R_2[\delta_{NCC}(29) + \delta_{ONC}(13)] + R_1[\delta_{CCC}(13) + \delta_{CCN}(12)]$
12	248	215	254		$R_1[\tau_{CCNN}(35)] + R_1[\tau_{CCCC}(11)]$
11	220	195	203		$R_1[\tau_{CCCC}(62)] + R_2[\tau_{CCCC}(10)]$
10	192	191	190		$R_2[\delta_{NCC}(17)] + (R_1 + R_2)[\nu_{NC}(12)] + R_1[\delta_{CCN}(10)]$
09	187	186	179		$R_1[\tau_{CCCC}(37) + \gamma_{OCCC}(21) + \gamma_{CCCC}(21)]$
08	171	158	168		$(R_1 + R_2)[\nu_{NC}(11)] + R_1[\delta_{CNN}(10)] + R_2[\delta_{NCC}(10)]$
07	156	83	146		$(R_1 + R_2)[\tau_{CNNC}(13)]$
06	78	73	119		$(R_1 + R_2)[\tau_{CCCC}(42)] + R_1[\tau_{CCNN}(10)]$
05	57	59	72		$R_2[\tau_{ONCC}(39) + \delta_{NNC}(17)] + R_1[\delta_{CNN}(12)]$
04	53	57	61		$R_2[\tau_{ONCC}(53) + \delta_{NNC}(14)]$
03	34	31	55		$R_1[\tau_{HCCC}(26)] + \tau_{CNNC}(25) + R_2[\gamma_{NCCC}(12)]$
02	28	19	31		$R_1[\tau_{HCCC}(29)] + \gamma_{CCCC}(11)] + R_2[\tau_{NNCC}(11)] + \tau_{CNNC}(10)$
01	14		22		$R_2[\tau_{NNCC}(62)]$
R^2 =	0.999	0.918	0.999		
RMSD=	19.08	198.76	20.40		

[a] Taken from [24]. [b] PED less than 10% are not shown. ν, Stretching; δ, bending; γ, out of plane bending; τ, torsion modes; sym, symmetric; asym, anti symmetric; Me, methyl; w, weak; m, medium; s, strong; v, very; sh, shoulder; br, broad.

Table 4. The stretching vibrations and theoretical frequencies on (O–H···N) structure for the title compounds

	Azo form		Transition state		Hydrazo form	
	calculated frequencies (cm^{-1})	assignments and (PED%)	calculated frequencies (cm^{-1})	assignments and (PED%)	calculated frequencies (cm^{-1})	assignments and (PED%)
NAB-1	3078	ν[24O–25H] (92)	1838	ν[21N···25H] (17)	3105	ν[21N···25H] (93)
			1365	ν[24O···25H] (39)		
			1365	ν[21N···25H] (27)		
			564	ν[21N···25H] (19)		
			564	ν[24O···25H] (19)		
NAB-2	3155	ν[21O–22H] (98)	1845	ν[20N···22H] (15)	3101	ν[20N–22H] (89)
			1406	ν[21···22H] (46)		
			1406	ν[20N···22H] (32)		
			564	ν[20N···22H] (18)		
			564	[21O···22H] (14)		

Table 5. Calculated chemical shift values (with respect to TMS) of the tautomeric forms with GIAO method and experimental data for *NAB*-1 molecule

Atoms	Experimental[a] (ppm) *NAB*-1 (solvent: DMSO)	Calculated B3LYP/6-311G(*d*) basis set GIAO method			
		azo form		transition state	hydrazono form
		(solvent: DMSO)	(solvent: none)	(solvent: none)	(solvent: none)
1-C	103.11	105.77	104.14	104.94	107.78
2-C	154.47	165.06	164.97	177.06	184.12
3-C	133.36	140.34	139.54	140.41	140.24
4-C	129.13	144.98	144.33	141.73	142.24
5-C	110.32	114.11	112.94	114.88	120.40
6-C	164.97	172.41	170.77	172.95	173.86
10-C	158.66	162.19	160.83	156.74	152.92
11-C	122.22	134.53	133.13	126.91	120.31
12-C	122.22	118.69	117.94	119.06	117.77
13-C	124.86	131.13	129.90	130.20	130.49
15-C	124.86	130.41	129.60	130.31	130.92
17-C	147.12	156.13	154.99	153.86	152.04
	R^2 =	0.948	0.946	0.922	0.846
	RMSD =	8.249	7.488	8.877	10.993
7-H	6.385	6.243	5.938	5.841	5.506
8-H	7.677	7.930	7.826	7.471	7.010
9-H	6.539	6.763	6.658	6.512	6.367
14-H	8.017	7.869	7.631	7.310	6.895
16-H	8.017	8.077	8.011	8.061	7.881
18-H	8.337	8.439	8.363	8.280	8.235
19-H	8.337	8.378	8.326	8.317	8.315
23-H	12.300	5.342	4.458	4.547	4.335
25-H	10.800	11.640	11.625	21.133	14.646
	R^2 =	0.983	0.977	0.828	0.910
	RMSD =	0.331	0.365	3.668	1.471

[a] Taken from [24].

Table 6. Calculated chemical shift values (with respect to TMS) for the tautomeric forms of *NAB*-2 molecule with GIAO method

Atoms	Calculated B3LYP/6-311G(*d*) basis set GIAO method		
	azo form	transition state	hydrazono form
1-C	113.18	116.01	120.79
2-C	162.96	176.37	184.39
3-C	131.10	132.72	132.55
4-C	165.84	163.41	161.71
5-C	109.06	105.80	105.38
6-C	161.88	165.33	164.83
9-C	160.72	155.96	152.26
10-C	133.36	126.75	120.41
11-C	116.80	117.77	116.17
12-C	130.16	130.56	130.85
14-C	129.76	130.40	131.02
16-C	154.94	153.62	151.92
26-C	25.02	25.90	25.91
7-H	6.245	6.174	5.890
8-H	6.357	6.051	5.758
13-H	7.631	7.297	6.908
15-H	7.714	7.822	7.597
17-H	8.373	8.293	8.254
18-H	8.334	8.329	8.327
22-H	10.997	21.196	14.584
27-H(methyl)	2.496	2.460	2.287
28-H(methyl)	2.557	2.460	2.287
29-H(methyl)	1.959	1.966	1.876
31-H	7.024	6.452	6.085

and belongs to the C_1 point group. The symmetry species of all the vibration modes for both the two compounds are written in Tables 2 and 3. In the tables are also given the assignments of all the fundamental vibration modes obtained by using VEDA 4 programs. For C–H (aromatic) stretching, the frequencies values were computed at the ranges of 3051–3108 cm^{-1} for *NAB*-1 and 3070-3108 cm^{-1} for *NAB*-2, with the highest percentile (% PED). Also, N=N stretching mode were calculated as 1477 and 1473 cm^{-1}, for *NAB*-1 and *NAB*-2, respectively. In an earlier study, N=N stretching mode for azobenzene was observed at 1511 cm^{-1} by Zimmermann et al. [28]. Furthermore, Kalra *et al.* reported that the peaks observed at 1345 cm^{-1} and 1515 cm^{-1} were due to symmetric and asymmetric streching vibrations of $-NO_2$ group, respectively, in an experimental study carried on a nitroazobenzene derivative [29]. In our computations, O–N stretching modes were obtained as 1322 and 1532 cm^{-1} for each two molecules.

The correlation values (R^2) between the experimental and calculated frequencies can be seen in the last lines of Tables 2 and 3. The mean root-mean-square deviation (RMSD) is a quantity used to measure how close forecasts or predictions are to the eventual outcomes in statistics. So, these calculations are also used between the experimental and theoretical (azo-hydrazo and TS form) frequencies. The statistics results show that the agreements with experimental data are better level for hydrazo form in Table 2 and for azo form in Table 3 than their other forms. Besides, the OH and NH stretching vibrations in O–H···N interaction are given in Table 4.

3.4. Chemical Shifts

The calculated ^1H and ^{13}C NMR chemical shifts (with respect to TMS) for all the forms of the title compounds are tabulated in Tables 5 and 6. The experimental chemical shift values for the *NAB*-1 in Table 5 have been obtained from Spectral Database for Organic Compounds Web Page [24]. But it was not found for the *NAB*-2 in the literature. ^1H NMR (in $CDCl_3$) of the aromatic structure–NO_2 have been reported as 7.96–8.37 ppm for a similar compound in a study of synthesis and properties of new ionic liquid crystals based on para-nitroazobenzene [30]. In our study, we calculated the ranges of 7.869–8.439 ppm and 7.631–8.373 ppm for azo form of *NAB*-1 and *NAB*-2, respectively. Consequently, the correlation factors between the experimental and theoretical chemical shifts can be seen in the last lines of the table. According to these values it can be stated that the agreement between the experimental and calculated chemical shifts is good.

4. CONCLUSIONS

In this study, the most stable tautomeric forms of *NAB*-1 and *NAB*-2 compounds were investigated. It was found as hydrazo form for *NAB*-1 and azo form for *NAB*-2. Besides, the theoretical vibrational frequencies, ^1H and ^{13}C NMR chemical shifts and the frontier-second frontier molecular orbital energy values for the ground state conformers of the compounds were obtained by using density functional theory (DFT/B3LYP) method with 6-311G(*d*) basis set. All the assignments of the theoretical frequencies were obtained by potential energy distribution (PED) analysis. Generally, it can be said that the calculated results of the compounds were to be in a good agreement with the experimental data. Some incompatibility of the calculations with the experimental data can be attributed that the molecular geometries in the gas phase may be different from the one in the solid phase, owing to extended hydrogen bonding and stacking interactions.

REFERENCES

1. H. Zollinger, *Color Chemistry: Synthesis, Properties, and Applications of Organic Dyes and Pigments* (Wiley-VCH, Weinheim, 1991).
2. J. L. Humphrey, K. M. Lott, M. E. Wright, and D. Kuciauskas, J. Phys. Chem. B **109**, 21496 (2005).
3. S. K. Yesodha, C. K. S. Pillai, and N. Tsutsumi, Prog. Polym. Sci. **29**, 45 (2004).
4. J. L. Zhou, X. F. Chen, X. H. Fan, C. X. Lu, and Q. F. Zhou, J. Polym. Sci. A: Polym. Chem. **44**, 6047 (2006).
5. N. Li, J. Lu, Q. Xu, and L. Wang, Opt. Mater. **28**, 1412 (2006).
6. K. Ichimura, Chem. Rev. **100**, 1847 (2000).
7. M. Azuki, K. Morihashi, T. Watanabe, et al., J. Mol. Struct. (Theochem) **542**, 255 (2001).
8. P. L. Tarifa, G. S. Sanz, I. Alkorta, et al., J. Mol. Struct. **1015**, 138 (2012).
9. R. Gup, B. Krkan, and E. Giziroglu, Dyes Pigments **73**, 40 (2007).
10. F. Karci and F. Karci, Dyes Pigments **77**, 451 (2008).
11. M. Bella, V. Milata, C. López, et al., Spectrosc. Lett. **46**, 91 (2013).
12. S. Mishra and P. Tandon, Mol. Simulat. **38**, 872 (2012).
13. Y. Dimitrova, Spectrosc. Lett. **43**, 282 (2010).
14. D. C. Young, *Computional Chemistry: A Pratical Guide for Applying Techniques to Real-World Problems* (Wiley, New York, 2001).
15. J. R. Cheeseman, G. W. Trucks, T. A. Keith, et al., J. Chem. Phys. **104**, 5497 (1996).
16. T. A. Keith and R. F. W. Bader, Chem. Phys. Lett. **210**, 223 (1993).
17. R. Ditchfield, Mol. Phys. **27**, 789 (1974).
18. C. M. Rohlfing, L. C. Allen, and R. Ditchfield, Chem. Phys. **87**, 9 (1984).
19. M. J. Frisch, G. W. Trucks, H. B. Schlegel, et al., *Gaussian 03*, Revision C.02 (Gaussian Inc., Pittsburgh, PA, 2003).
20. M. H. Jamroz, *Vibrational Energy Distribution Analysis*, VEDA 4 Computer Program, (Warsaw, 2004).
21. A. Frisch, A. B. Nielsen, and A. J. Holder, *Gauss View User Manual* (Gaussian Inc., Pittsburgh, 2001).
22. C. Peng and H. B. Schlegel, Israel J. Chem. **33**, 449 (1993).
23. C. Peng, P. Y. Ayala, H. B. Schlegel, et al., J. Comp. Chem. **17**, 49 (1996).
24. http://riodb01.ibase.aist.go.jp/sdbs/cgi-bin/cre_index.cgi?lang=eng
25. http://www.sigmaaldrich. com/european-export.html
26. I. Fleming, *Frontier Orbitals and Organic Chemical Reactions* (Wiley, London, 1976).
27. K. Fukui, Science **218**, 747 (1982).
28. F. Zimmermann, T. H. Lippert, C. H. Beyer, et al., Appl. Spectrosc. **47**, 986 (1993).
29. N. Kalra, D. K. Chaturvedi, S. Kumar, et al., Ind. J. Pure Appl. Phys. **45**, 618 (2007).
30. Q. Zhang, K. Wang, Q. Ren, et al., Liq. Cryst. **38**, 1349 (2011).